Three-dimensional crack monitoring by electrical resistivity measurement.

Anatja Samouëlian, Guy Richard, Isabelle Cousin, Roger Guerin, Ary Bruand, Alain Tabbagh

Three-dimensional crackmonitoring by electrical Resistivity measurement

A. SAMOUE LIAN [a], G. RICHARD [b], I. COUSIN [a], R. GUERIN [c], A. BRUAND [d] and A. TABBAGH [c]
[A] INRA, Unite´ de Science du Sol, BP 20619, 45166 Ardon,
[B] INRA Unite´ d'Agronomie, rue Fernand Christ, 02007 Laon,
[C] UMR 7619 « Sisyphe », Case 105, 4 place Jussieu, 75005 Paris,
[D] ISTO, UMR 6113 CNRS-UO, Université d'Orléans, Géosciences, BP 6759, 45067 Orléans Cedex 2, France

Summary
Soil cracks formed by natural processes play a key role in water and gas transfer. Patterns of soil cracks are, however, difficult to characterize. Our aim here is to assess the effectiveness of three-dimensional electrical resistivity surveys in detecting soil crack networks. A three-dimensional electrical survey was carried out by a square array quadripole with Cu–$CuSO_4$ electrodes (electrode spacing of3 cm). The measurements were made with two orientations (0° and 90°) on a block (26 cm x 30 cm x 40 cm) of soil while it dried for 18 days under controlled conditions. Two indexes, calculated from the apparent resistivity values, were evaluated to detect the degree ofso il heterogeneity: (i) an anisotropy index based on the ratio between the apparent resistivity at 0° and that at 90° ; and (ii) the angle-array orientation corresponding to the preferential anisotropic orientation (maximum resistivity). The anisotropy index provided information on the presence of cracks and the orientation for crack width >1mm in the first pseudo-depth (i.e. depth of investigation), while the angle-array orientation provided information on crack extension for the whole pseudo-depth. Information about the presence, position, orientation and extension of cracks can be obtained from an analysis of apparent resistivity obtained by a three-dimensional electrical survey. Such direct analysis will help the resistivity inversion to detect the crack network.

Introduction

Cracking of soil is related to shrinking and swelling and plays a significant role in the transport of water and gas. The geometry of soil cracks is usually described by one- and two-dimensional analyses (Hallaire, 1988; Stengel, 1988; Ringrose-Voase&Sanidad, 1996), whereas three-dimensional description is required to relate the geometry of soil cracks to mass transfer characteristics (Vogel et al., 1993). The current methods available for the three-dimensional analysis of crack geometry are limited in various ways. As examples, the three-dimensional analysis of soil porosity by the study ofs erial sections (Cousin et al., 1996) is a destructive technique and requires the samples to be dried and impregnated with resin ; and X-ray tomography as used by Macedo et al. (1998) can be applied only to small samples under laboratory conditions. As a consequence, these techniques do not enable us to describe cracking dynamics when the soil dries or is rewetted. The geometrical analysis ofthe opening and closing of cracks requires a non-destructive method applicable both in the field and laboratory and on a wide range of volumes, thus enabling the study of crack geometry at different scales. Three-dimensional electrical prospecting is an emerging technique that can assess properties of both top- and subsoil non-destructively and at several scales. Using an adapted quadripole strategy, three dimensional electrical prospecting enables one to make the measurements directly over a wide range of soil volumes and to make three-dimensional analysis of their characteristics (Tabbagh et al., 2000). Three-dimensional electrical resistivity surveys are commonly collected by a network of in-line survey arrays, such as Wenner, Schlummberg, or Dipole-Dipole arrays (Xu & Noel, 1993; Oglivy et al., 1999; Zhou et al., 2002). Meheni et al. (1996) emphasize that the resulting apparent resistivity maps vary according to array orientation and electrical discontinuities. Indeed, asymmetric bodies and anisotropic materials exhibit different behaviours depending on which direction the current passes through them (Scollar et al., 1990). This is all the more true for a medium having contrasted resistivities, such as cracked soil. In this case, the electrical current does not encounter the same resistance when it passes perpendicularly to, or parallel with, resistant bodies such as cracks. Indeed, apparent resistivity

depends on the location and orientation of the current source relative to the body under study (Bibby, 1986). Chambers et al. (2002) emphasized that in a heterogeneous medium, three-dimensional electrical resistivity model resolution was sensitive to the orientation of the electrode configuration. Habberjam & Watkins (1967) showed that the square array provides a measurement ofresistiv ity less dependent on orientation than that given by an in-line array. Previous work by Samouelian et al. (2003) emphasizes the need for significant advances in the mathematical inversion of apparent resistivity relating to electrical heterogeneities such as cracks. So we can get more accurate three-dimensional inversion in a context of soil cracking, we have chosen to improve the acquisition of three dimensional electrical resistivity data by using a square array quadripole.

This work is part ofa study that aims to monitor the spatial and temporal progression of the soil cracking pattern by three dimensional electrical resistivity prospecting. We first assess the ability to detect soil cracks through three-dimensional apparent electrical resistivity, before focusing on the progression of the soil cracking pattern during drying.

Materials and methods

Soil

The experiment was done on a soil block (x = 26 cm, y = 30 cm, z = 40 cm) collected at the INRA Experimental Centre at Mons-en-Chaussée (Somme, France). The soil, formed from loess, is an orthic Luvisol (Richard et al., 2001). The soil block was sampled from the surface in a place where the soil had been compacted by traffic under wet conditions. The soil was initially massive with a volumetric water content of 0.43 and a bulk density of 1.60 g cm^{-3}. The experiment was done during summer, and the sample, enclosed in a box, dried out through the upper surface only. The soil block was dried for 18 days : in the afternoon for 4 hours daily in the open air and then in the laboratory at controlled conditions of both temperature (20–22°C) and relative humidity (55–65%) for the rest of the time. After a drying period of 18 days, the volumetric water content was 0.34. During the drying, air-filled porosity increased, with cracks appearing at the soil surface and spreading downwards. The measurements were taken in the morning either daily or every two days according to crack development to record electrical resistivity measurements at similar temperatures. In this way, we obtained a set of 12 electrical resistivity measurements over the 18-day drying period.

The principles of the three-dimensional electrical measurement

We used a pair of near-orthogonal current source electrode arrays to acquire the three-dimensional resistivities. This type of square quadripole avoids directional preferences introduced by an in-line electrode layout. As shown in Figure 1(a), the current electrodes A and B and potential electrodes M and N are not on the same line of measurement but on two parallel lines, so that they form a square. For each square two electrode configurations were used at 90° to each other. The first pseudo-depth (i.e. depth of investigation) was recorded at the shortest inter-electrode spacing a (Figure 1b). When the inter electrode spacing increased by a to 2a, the measurements corresponded to the second pseudo-depth investigation. As the inter-electrode spacing increased to 3a, 4a, 5a, 6a and 7a, the corresponding pseudo-depth was, respectively, 3, 4, 5, 6 and 7. For each spacing, the maximum number of squares was used within the 8x8 grid – i.e. 49 for the smallest spacing and 1 for the largest (Figure 1b). The number of data decreased as the depth increased, i.e. when the inter-electrode spacing increased. The apparent electrical resistivity (p) measurements corresponding to the array orientation α = 0° or 90° were denoted $p_{0°}$ and $p_{90°}$, respectively, and expressed in Ωm.

The experiment was performed by eight inline Cu–$CuSO_4$ electrodes installed in the central part ofthe 8x8 grid with a spacing of 3 cm. As a consequence the measurement area was 21 cm x 21 cm. The minimum inter-electrode spacing a was 3 cm, which was judged from a previous experimental display by Samouelian et al. (2003) to be adequate for detecting cracks 1mm wide. Cracks were detected by their resistive electrical signal compared with boxing. All the measurements were taken with specific electrodes, manufactured from small, saturated, cone-

shaped ceramic cups (2mm external diameter) linked to a Cu–$CuSO_4$ complex as proposed by Samoue¨ lian et al. (2003). The copper wire had a section of 0. 6mm, and the concentration of the $CuSO_4$ solution was 0.05M. The ceramic cup was joined to a transparent plastic rigid tube (3mm external diameter and 2mm internal diameter). The saturated ceramic cup placed on the soil surface facilitated a wet contact at given points. Measurements were made with a programmable multi-electrode system (Multinode) and a resistivity meter (Syscal R1 Plus, Iris Instrument, Orléans). The experiment lasted 41 minutes. It resulted in 280 measurements distributed among seven pseudodepths. Each pseudo-depth contained the electrical resistivity related to $p_{0°}$ and $p_{90°}$ acquisition. Thus one half of the total number of acquisitions for each pseudo-depth corresponded to $p_{0°}$, and the other half to $p_{90°}$. The first pseudo-depth (electrode interspacing a = 3 cm) comprised 98 measurements, 49 of them corresponding to $p_{0°}$ and 49 to $p_{90°}$. The other pseudo-depths studied had electrode interspacing of6, 9, 12, 15, 18 and 21 cm and contained, respectively, 72, 50, 32, 18, 8 and 2 measurements. The seventh pseudo-depth was not taken into account because it contained only two values, one for each array orientation.

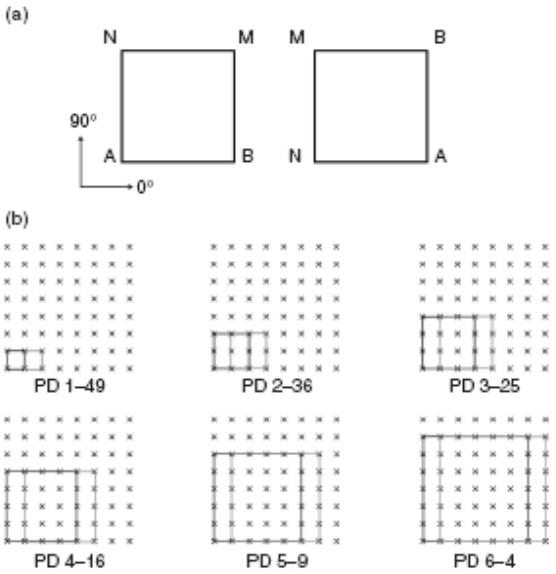

Figure 1 Square array configuration: (a) the location of the current (A and B) and potential (M and N) electrodes for the two array orientation and (b) inter-electrode spacing corresponding to the different pseudo-depths PD1 to PD6, with the number of acquisitions for each square array orientation specified.

Results and discussion

Description of the crack network at the soil surface at the end of the experiment Figure 2 shows the cracking network pattern after desiccation at the end of the experiment. The top surface of the block was divided into square areas 3 cmx3 cm numbered from 1 to 49. The length of the area side corresponded to the smallest inter electrode spacing (a¼3 cm), i.e. the electrode square array position for the first pseudo-depth. The cracks had various widths, lengths and orientations (Figure 2). We determined the mean crack width (mm) and the area proportion within each unit area. The binary photography showed the cracks in black and the solid parts in white. We evaluated the mean crack width for each unit area by manually counting the number of pixels perpendicular to the crack direction, and we calculated the crack proportion by comparing the proportion of black pixels to white ones. As expected, crack width increased with the proportion of surf ace cracks and the two variables were closely related (r = 0.93, n = 49). The three widest cracks were linked to the major triple point located in unit area 19 (Figure 2).

Overall description of the change in 3D apparent resistivity data

The mean apparent resistivity and the median, minimum, maximum, and the standard deviation were calculated for each set of data corresponding to each of the six pseudo depths (PD1 to PD6) at the initial and final stages and the two array directions ($p_{0°}$ and $p_{90°}$) (Table 1). At the initial stage, the mean and the median increased slightly with pseudo-depth whatever the direction of the array. We attribute this slight increase to side-effects during measurement that may have been caused by the small thickness of the soil sample compared with the wide inter-electrode spacing. The standard deviation remained small and similar for pseudo-depths PD1 to PD5, and was even smaller for pseudo-depth PD6 (Table 1). Maximum and minimum values of *p* were 54 and 12Ωm, respectively. At the final stage, the mean and median varied less as a function of pseudo-depth than at the initial stage and there was no progressive increase from PD1 to PD6. Maximum and minimum *p* values of 128 and 6Ωm, respectively, were from the first pseudo-depth. The mean apparent resistivity for all the pseudo-depths and for the two array orientations was 27Ωm for the initial stage and 44Ωm for the final stage. The values of r recorded at the initial and final stages are plotted in Figure 3 with respect to the pseudo-depth. Compared with the initial stage, r was more variable. Such dispersion of the *p* values indicates the emergence of electrical heterogeneities.

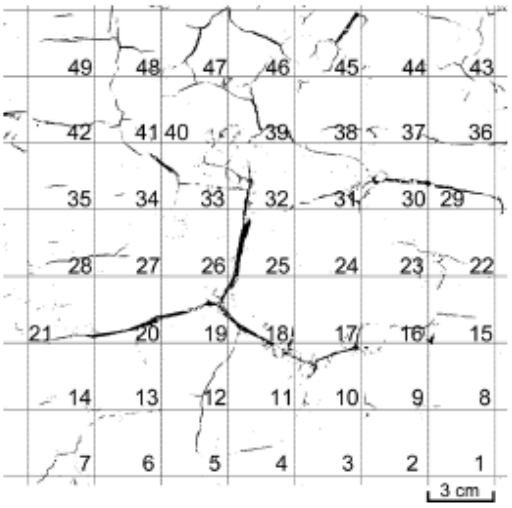

Figure 2 Binary image of the top surface of the block showing the cracking network pattern after desiccation at the end of the experiment. The grid nodes correspond to the electrode position and the square cells to the unit areas for the first pseudo-depth.

Spatial distribution of three-dimensional apparent resistivity at the end of the experiment

Figure 4 shows horizontal sections of r values at each pseudo depth at the end of the experiment and for the two array orientations. Each *p* measurement was attributed by convention to the geometric centre point of the square array shown in Figure 1. Though the soil volume investigated increased with the pseudo-depth, the size of the representative maps decreased because the acquisition quadripoles are overlapped with depth, and the unit area representation remained constant (Figure 1). The patterns of resistivity displayed in the sections corresponding to the two array directions are different. Indeed, a large r for one array orientation usually corresponds to a small *p* for the other. The variation of *p* corresponds to local *p* anomalies. The shapes of the anomalies are roughly similar at pseudo-depths 1–5 when recorded with one array direction. The two resistivity patterns were similar for the sixth pseudo depth.

final stages for the six pseudo-depths

		Initial stage						Final stage					
		PD1	PD2	PD3	PD4	PD5	PD6	PD1	PD2	PD3	PD4	PD5	PD6
$\rho_{0°}$	Mean	21	26	31	36	40	44	44	43	44	52	53	58
	Median	21	25	30	35	40	44	43	39	40	53	57	59
	Minimum	14	20	26	31	36	44	6	21	31	31	36	55
	Maximum	34	37	40	41	45	46	128	91	73	75	69	61
	SD	4	3	3	3	3	1	26	16	12	13	10	2
$\rho_{90°}$	Mean	19	24	28	35	43	53	47	47	40	42	51	58
	Median	19	23	28	34	41	52	41	41	41	35	44	56
	Minimum	12	18	22	28	39	51	9	10	16	25	37	56
	Maximum	25	28	36	42	51	54	108	108	65	67	76	61
	SD	3	3	4	4	4	1	27	16	14	14	14	2
AAI	Mean	1.16	1.13	1.12	1.05	0.95	0.85	1.71	1.58	1.41	1.47	1.15	1.00
	Median	1.07	1.13	1.06	1.03	0.97	0.84	1.06	1.18	0.92	1.48	1.29	1.04
	Minimum	0.57	0.80	0.73	0.74	0.71	0.82	0.07	0.38	0.50	0.48	0.47	0.90
	Maximum	2.57	1.67	1.84	1.35	1.16	0.89	9.63	7.54	4.64	2.84	1.86	1.08
	SD	0.43	0.24	0.25	0.20	0.14	0.03	2.01	1.51	1.08	0.78	0.43	0.08
α_{max}	Mean	43	42	42	44	48	50	46	42	43	40	43	46
	Median	45	40	45	45	45	50	45	40	45	35	40	45
	Minimum	20	30	30	35	40	50	5	10	10	20	30	45
	Maximum	60	50	55	55	55	50	85	70	65	65	65	50
	SD	10	6	6	6	6	0	24	18	15	16	12	2

Table 1 Mean, median, minimum, maximum and standard deviations (SD) of $p_{0°}$, $p_{90°}$, apparent anisotropic index (AAI) and α_{maxx}, at the initial and final stages for the six pseudo-depths

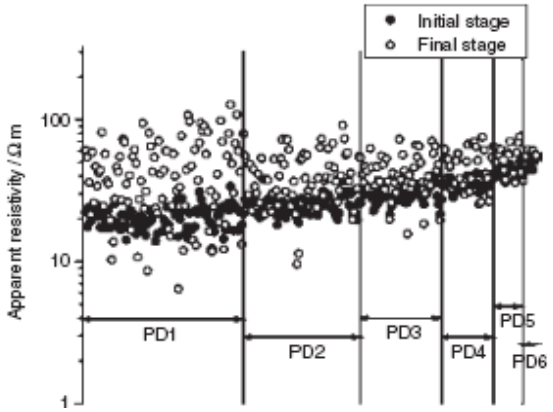

Figure 3 Initial and final measurement distributions for the six pseudodepths.

We assumed that the complementary distribution of apparent resistivity was related to the change of the soil structure due to drying. Indeed at the final stage air-filled porosity increased and a crack network appeared at the soil surface. Using the two array orientations $\alpha = 0°$ and $\alpha = 90°$, we calculated a dimensionless apparent anisotropic index (AAI) as follows :

$$\mathrm{AAI} = \frac{\rho_{0°}}{\rho_{90°}}.$$

The determination ofthe electrical anisotropy index proved suitable since it highlighted the presence of heterogeneity. It also enabled the electrical resistivity measurements to be summarized on a single map for each pseudo-depth (Figure 5). When $p_{0°}$ and $p_{90°}$ are similar, AAI

is close to 1 and the soil volume investigated is homogeneous, and there is no electrical heterogeneity. The major anisotropic zones were indicated by large and small AAI. As expected, they were found more at the soil surface than at depth: AAI ranged from 0.07 to 9.63 at pseudo-depths 1, 2 and 3. Minimum AAI increased with pseudo-depth whereas maximum AAI decreased with it (Table 1), because the size of the array was probably larger than the extent of the cracks.

Using the apparent anisotropic index for crack detection

In terms of electrical resistivity, cracks are anisotropic discontinuities in the electrical field. As a consequence, AAI can be considered as an indicator for crack detection. We calculated the average AAI at the final stage and the mean crack width for each unit area by using the crack network shown in Figure 2. The cracks that did not cross the in-line measurement MN were also taken into account. The in-line measurement MN represented the space between the electrodes M and N where electrical potential is measured. Figure 6 shows the variation of AAI with respect to mean crack width per unit area. When AAI=1, the soil volume investigated was isotropic ; when AAI $\neq$ 1, the volume contained anisotropic electrical heterogeneities. When crack width was >1 mm, AAI values were either larger than 2.83 or less than 0.42 (Figure 6). These two thresholds are linked ; indeed one is the inverse ratio of the other. The first threshold was called I_{csup} and the second one $I_{cinf.}$ Most cracks with a width <1 mm, including all those that did not cross the MN in-line measurements, had an AAI value, between I_{cinf} and I_{csup}. The limited extent of such cracks laterally and with depth does not lead to strong electrical heterogeneity.

We also examined the relation between AAI and preferential crack orientation (Figure 7). Three cases were distinguished : (i) when the crack had a preferential orientation close to 90°, AAI>1, (ii) when the orientation was close to 45°, AAI$\cong$1, and (iii) when the orientation was close to 0°, AAI<1.

We constructed the map in Figure 8 by considering that elements with I_{cinf}<AAI<I_{csup} had no crack recognizable with the electrode interspacing and array geometry used in this study. For unit areas with AAI<I_{cinf} or AAI>I_{csup}, cracks were considered to be present and to be separated according to their preferential orientation (α = 0° or 90°). Cracks oriented at 45° were not detected, because their AAI was included within I_{cinf} and I_{csup}. Comparison of the crack network pattern shown in Figure 2 (the cracks not crossing the in-line measurement MN are excluded) with this map of AAI for each units shows that the triple point is clearly recognized at the limit of three zones with two distinct cracking orientations. Moreover, AAI values reflected the orientation of main cracks that were recognized at the soil surface. However, cracks with $\alpha\cong$45°, as in unit areas 7, 46 and 47 (Figure 2), or cracks that do not cross the in-line measurement MN, as in unit areas 21, 28 and 49, were not detected. The AAI is directly calculated by the mean experimental data and as a consequence, the I_{cinf} and I_{csup} threshold values given in this paper cannot be applied to another soil or different experimental conditions. Moreover, I_{cinf} and I_{csup} were defined with regard to the soil surface photograph and our observations (Figure 6), and they were used for only the first pseudo-depth. Indeed, observation of the soil surface gave an initial approximation of the cracking network, which was linked for reasons of accuracy only to the first pseudo-depth, since this was the smallest soil volume studied.

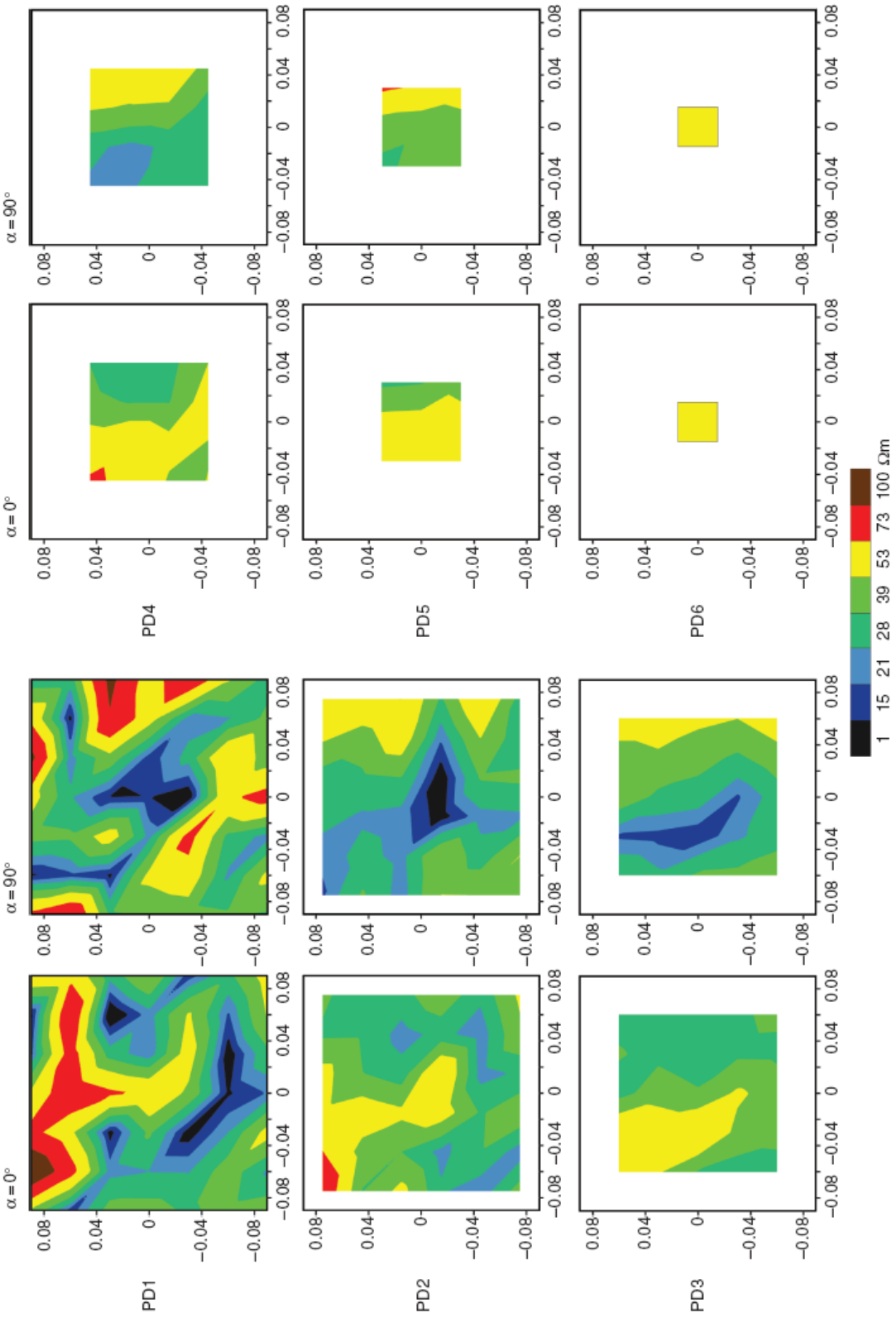

Figure 4 Apparent electrical resistivity distribution at the final stage.

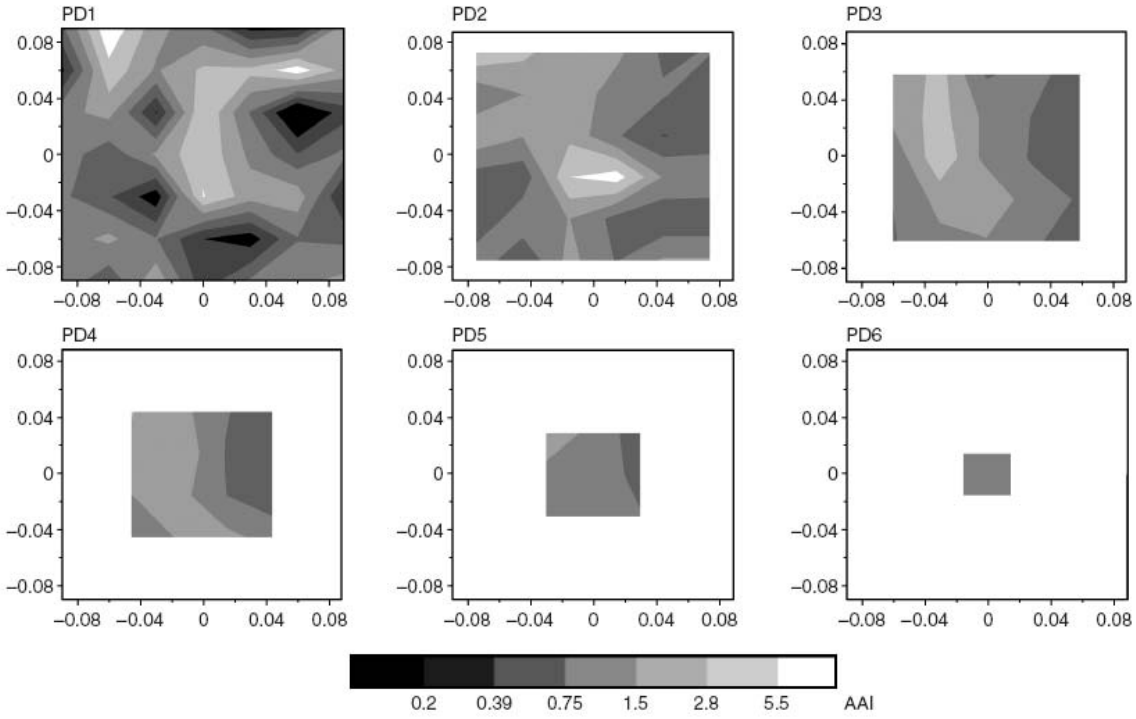

Figure 5 Spatial distribution of the apparent anisotropic index (AAI) at the final stage for the six pseudo-depths (PD1 to PD6).

Use of the preferential anisotropic orientation for crack detection

The AAI calculated from the first pseudo-depth data and I_{cinf} and I_{csup}, which were defined on the basis of surface observation, can be considered as an initial approximate description of the crack network. The apparent resistivity distribution is highly dependent on the orientation of the current source with respect to the anisotropy of electrical heterogeneity. To go further with our analysis, we calculated the array orientation corresponding to the maximum apparent resistivity values, α_{max}-array orientation. The primary data set was transformed by the rotation matrix **R** defined as follows :

$$\mathbf{R} = \begin{bmatrix} \cos\alpha & \sin\alpha \\ -\sin\alpha & \cos\alpha \end{bmatrix},$$

where α is the angle relative to the measurement grid. The resistivity values p_{α} and $p_{\alpha+90°}$ calculated using Equation (3) form our data set :

$$\begin{bmatrix} \rho_{\alpha} \\ \rho_{\alpha+90°} \end{bmatrix} = \mathbf{R} \begin{bmatrix} \rho_{0°} \\ \rho_{90°} \end{bmatrix}.$$

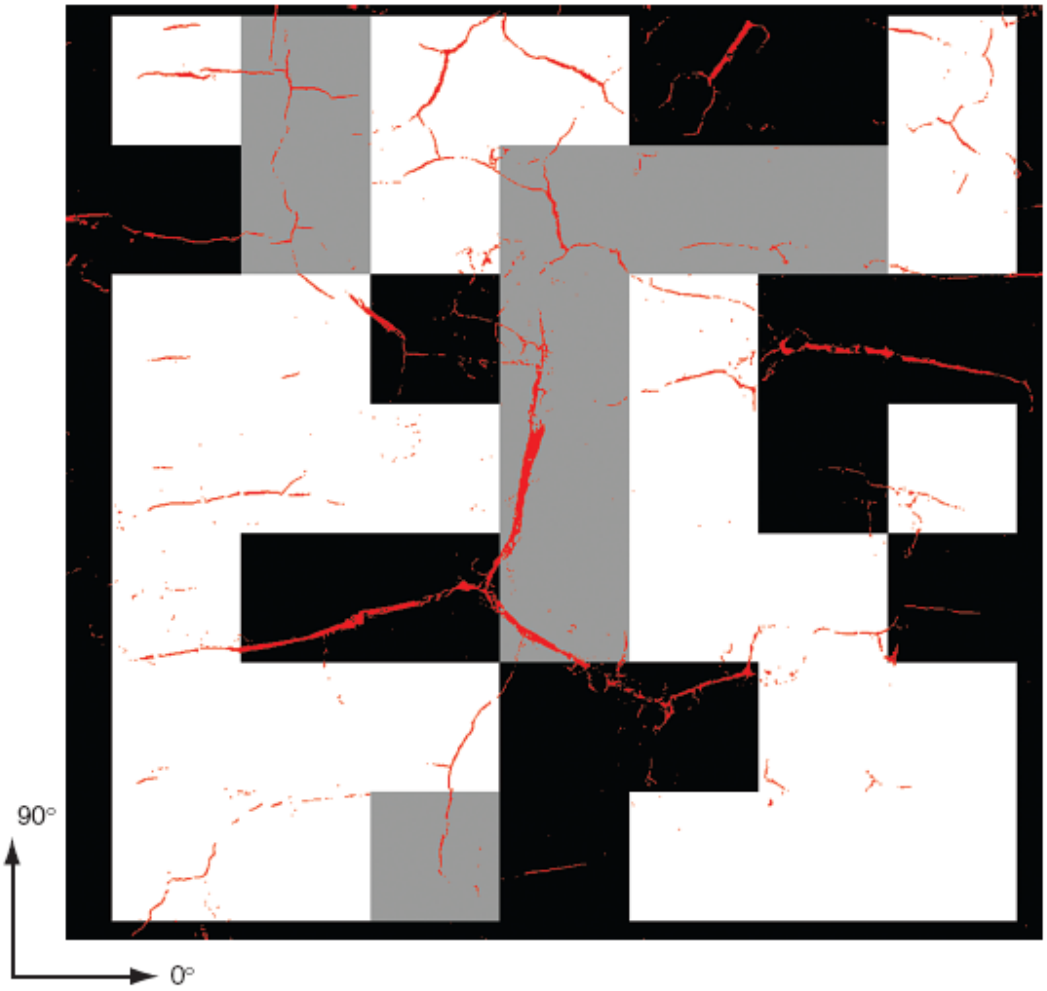

Figure 8 Mean crack orientation at the final stage : white squares represent units with Icinf<AAI<Icsup, grey squares represent units with AAI>Icsup, and black squares represent units with AAI<Icinf.

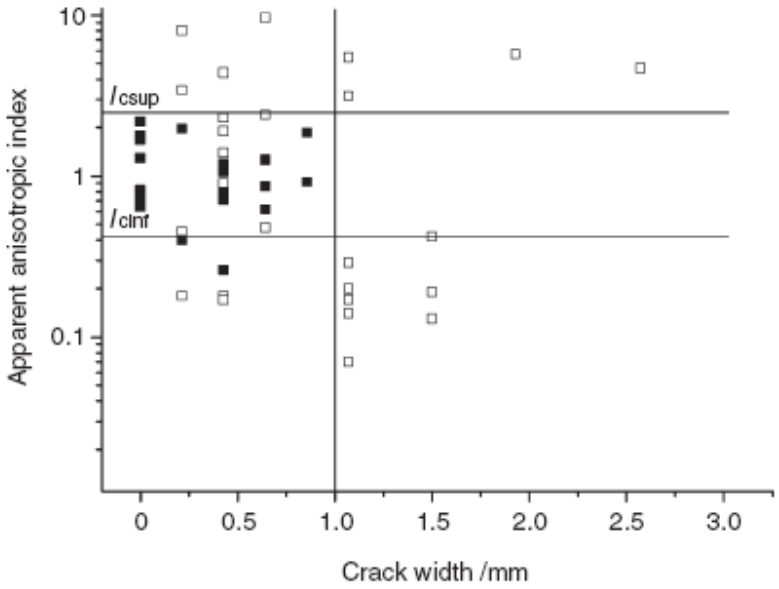

Figure 6 Variation ofthe apparent anisotropic index with respect to average crack width within each unit area: & cracks that do not cross and & cracks that cross the in-line MN (Icinf and Icsup are the two thresholds determined for crack identification >1 mm).

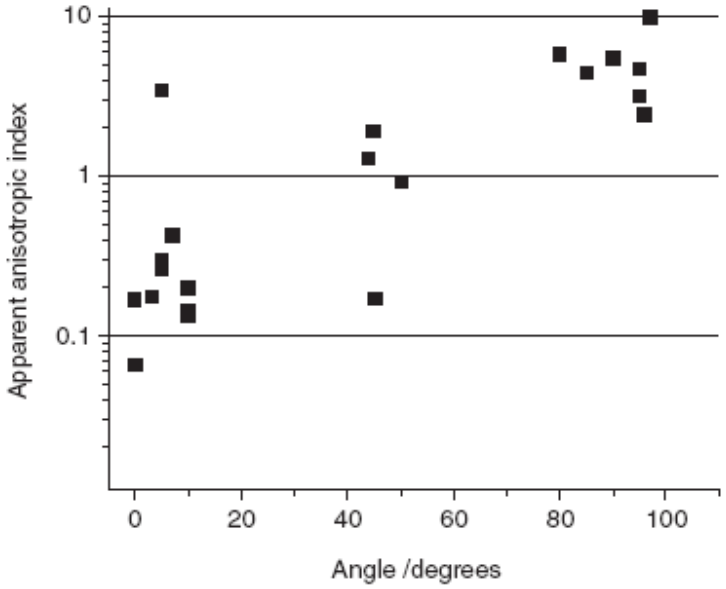

Figure 7 Anisotropic apparent index and main crack orientation.

These data were calculated for a values, at 5° intervals from 0° to 90°. The rotation matrix highlighted particular features such as the position and orientation of a resistivity discontinuity. Figure 9 shows the calculated apparent resistivity according to Equation (3) of three theoretical situations of apparent resistivities: $p_{0°} = p_{90°} = 27\Omega m$, $p_{0°} = 15\Omega m$ and $p_{90°} = 70\Omega m$, and $p_{90°} 70\Omega m$ and $p_{90°} = 15\Omega m$. In an isotropic medium ($p_{0°} = p_{90°}$), the maximum calculated apparent resistivity

value is recorded for α = 45°. In an anisotropic medium $p_{0°} \neq p_{90°}$)the maximum calculated resistivity value is recorded for $\alpha \neq 45°$. The crack is also oriented perpendicular to the value of α for which the apparent resistivity recorded is maximal. Thus, the value at αmax provides information on crack orientation. Based on calculations of αmax using an experimental data set we can conclude that, when α_{max} = 45°, the medium does not include anisotropic electrical heterogeneity ; and when $\alpha_{max} \neq 45°$, it includes anisotropic electrical heterogeneity whose orientations can be determined.
For our experimental dataset, we calculated α_{max} for each unit area and each pseudo-depth (Table 1). The results show that the mean α_{max} and its median were close to 45° whatever the pseudo-depth. On the other hand, the results also show that the range of α_{max} and its standard deviation decreased as the pseudo-depth increased. This indicates that α_{max} converged at 45° when the pseudo-depth increased, with a corresponding reduction of anisotropic electrical heterogeneity when the volume investigated increased. For the first pseudo-depth, the α_{max} values ranging between 40° and 50° corresponded to the unit areas where I_{cinf}<AAI<I_{csup} (Figures 5 and 10a) and can be considered as an isotropic medium. The α_{max} values ranging from 0° to 35° and from 55° to 90° corresponded to an anisotropic medium where cracks were present. The anisotropy directions illustrated in Figure 10(a) for the first pseudo-depth agree with the crack directions shown in Figure 8. The orientation of the electrical heterogeneity in unit areas 18, 19 and 11 agrees closely with the geometry of cracks linked to the major triple point. In unit areas 29 and 30, the orientations also correlated well with the crack orientation shown in Figure 8. Between the first and the second pseudo-depth, the orientation of electrical heterogeneity was preserved or shifted to 45° but never inverted. The third pseudo-depth showed a single major electrical heterogeneity oriented at 75° and located in three neighbouring unit areas. The following pseudo-depths, 4, 5 and 6, displayed an orientation α_{max} converging at 45°. In Figure 10(a), all the α_{max} values at the various pseudo depths were calculated for unit areas with a size corresponding to the smallest. However, the effective unit area increased with increasing depth, leading to overlapping of the area units. In Figure 10(b), the α_{max} values were calculated for areas corresponding to the unit area of the second pseudo-depth (36 cm2). Thus, four maps were required to represent all the apparent resistivity measurements at the second pseudo-depth. Only cracks >1mm were overwritten in Figure 10(b). The ringed crack in Figure 10(b) corresponded to the widest crack of the major triple point and showed a preferential orientation of 90_. Maps 1, 2, 3 and 4 show orientations of this crack at, respectively, 80°, 80°, 65° and 45°. Thus, in map 4 the unit area containing the major crack was not clearly identified as a crack since α_{max} = 45°. Generally, cracks >1mm are detected except when (i) crack orientation is equal to 45°, or (ii) cracks do not cross the MN in-line measurement. In these two cases, the unit area is not different from that of a non-cracked area.

When the inter-electrode spacing increased from *a* to 2*a* (second pseudo-depth), only the major cracks were distinguished. The widest cracks were detected down to the third pseudo-depth. Cracks spread downwards into the soil with a preferential orientation initiated from the surface. It can be assumed that as mean crack width increased, the corresponding crack depth increased also. As the pseudo-depth increased, the soil volume investigated also increased and the related influence of the cracks decreased. The electrical signal then became less disturbed by the heterogeneity.

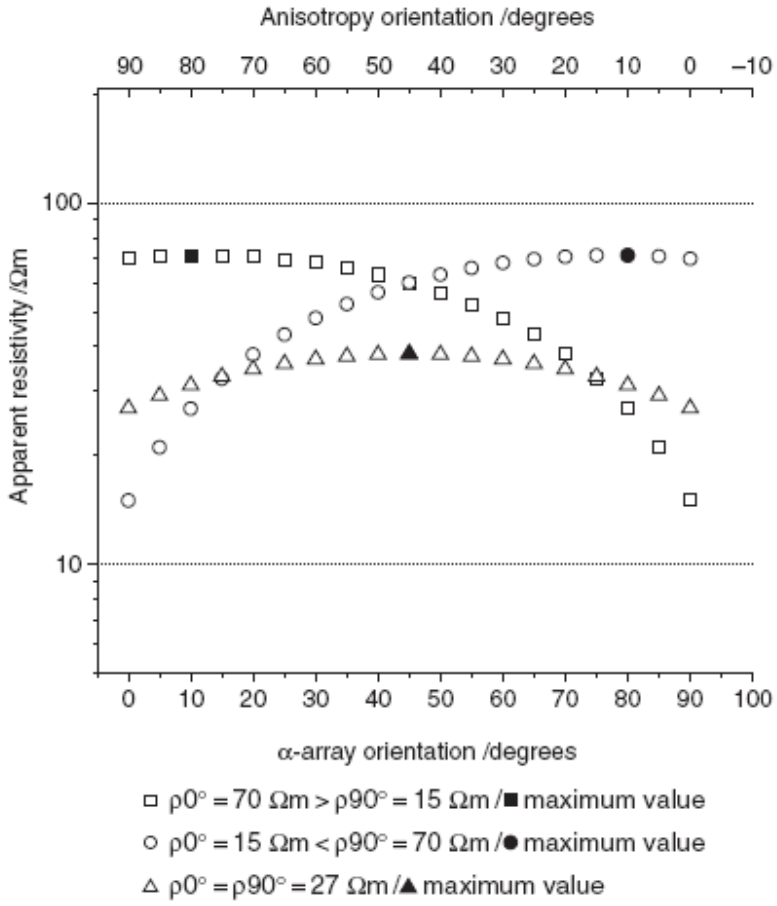

Figure 9 Variation of the apparent resistivity measurement with the square array orientation.

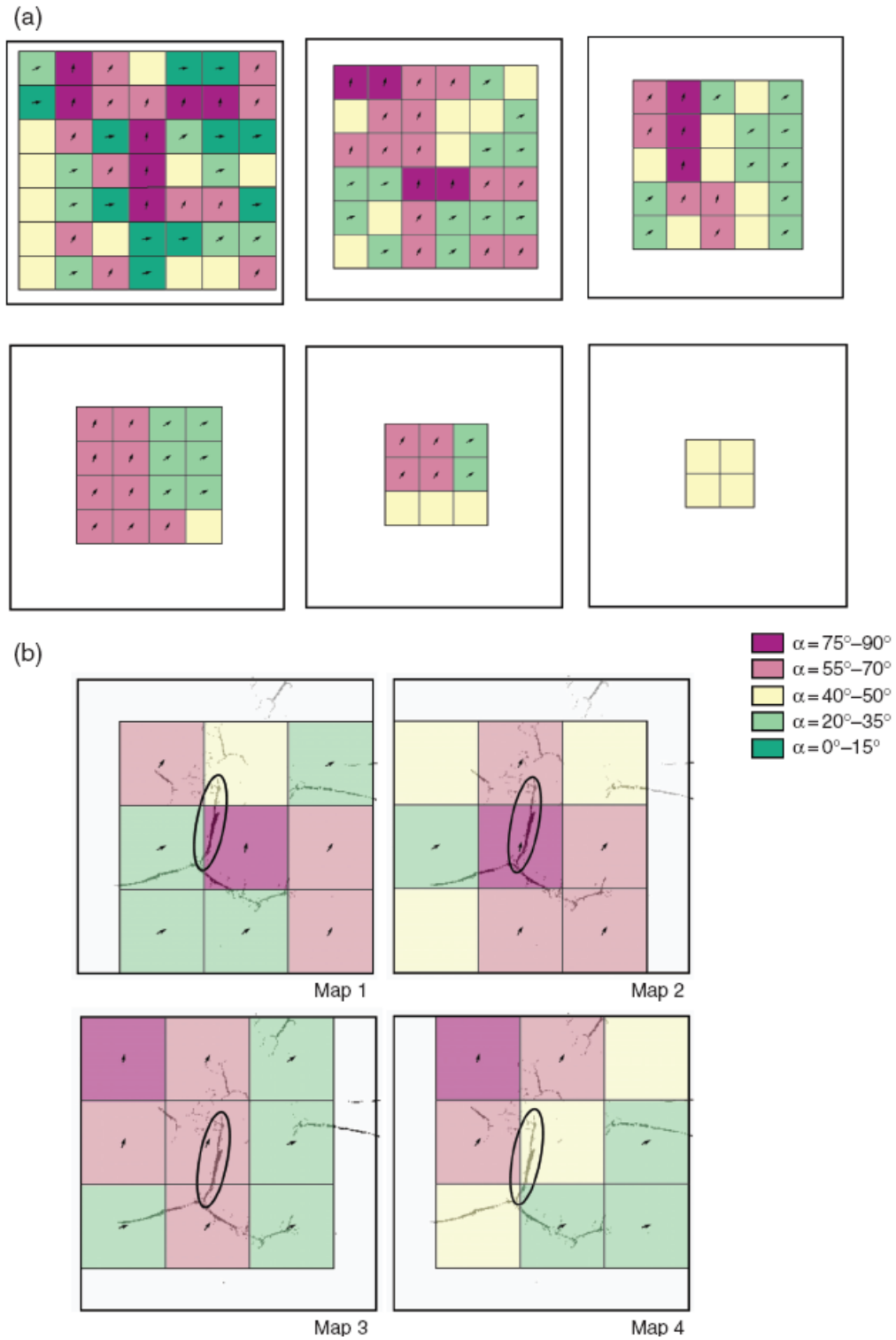

Figure 10 (a) Preferred anisotropy orientation for the six pseudo-depths at the final stage. (b) Details of the preferred anisotropy orientation for the second pseudo-depth; the ring outlines the widest crack of the triple point.

Temporal variation of the crack network pattern

By comparing the initial and final apparent resistivity values, we showed that the electrical resistivity method could detect the effect of drying on the soil block. Our results indicate that the distribution of electrical resistivity during the drying changes with both depth and time. Our analysis first focused on data from the first pseudo depth and on unit areas 19, 20 and 25 where major cracks were present, and unit area 24 where there was no crack at the final stage (Figure 2). At the final stage, the cracks within unit areas 19 and 20 had a preferred orientation close to α = 0°, whereas the crack within unit area 25 had a preferred orientation close to α = 90°. Unit area 24 with no crack showed no preferred orientation. The variations of $p_{0°}$ and $p_{90°}$ and of AAI during drying (18 days) for the four unit areas are presented in Figures 11 and 12. Variation of $p_{0°}$ and $p_{90°}$ showed that cracks in unit areas 19 and 25 were clearly initiated on the third day (Figure 11). Then, the apparent resistivity values changed suddenly between the third and the sixth day, $p_{0°}$ decreased as $p_{90°}$ increased in area 19, whereas variation was the opposite in area 25. In unit area 20, an apparent resistivity differentiation between $p_{0°}$ and $p_{90°}$ was observed from the fifth day. The crack had the same orientation as the crack in area 19. In fact, these two latter unit areas were adjacent, the crack observed in unit area 20 constituting the growth of the crack initiated in unit area 19. The cracks progressed and conserved their orientation through time. In unit area 24, $p_{0°}$ and $p_{90°}$ remained stable throughout the experiment. At the initial stage, the AAI values of the fourth unit area selected were between I_{cinf} and I_{csup}. From the third day AAI changed suddenly : it decreased from 0.70 to 0.16 in unit area 19, and increased from 1.6 to 4.7 in unit area 25. Both thresholds I_{cinf} and I_{csup} were exceeded, and the areas were also considered as cracking areas. The values of AAI in unit area 20 approached I_{cinf} from the fifth day. During the rest of the experiment, AAI oscillated around I_{cinf}. In unit area 24, AAI varied around 1 and never exceeded the thresholds. No crack was visible at the soil surface, in agreement with this observation. Thus, unit areas 19 and 25 on the one hand, and area 20 on the other, had two different cracking initiations. The first is abrupt and quick; it is related to the initiation of the triple point. The second crack initiation progressed more slowly and corresponded to the spread of on e arm of the triple point. Non-destructive acquisition through time permitted monitoring crack initiation, growth and extension.

As shown previously, the widest crack spread to the second pseudo-depth (Figure 10b). The orientation of preferential heterogeneities for two specific areas labelled A and B was monitored through time (Figure 13). The surface area corresponded to 36 cm2 and was related to the inter-electrode spacing at the second pseudo-depth. Area A corresponded to unit areas 17, 18, 24 and 25, whereas area B corresponded to unit areas 19, 20, 26 and 27. Thus area A included the main crack ofthe triple point at 90°, and area B the left arm of the triple point oriented at 0°. At the initial stage α_{max} of the two areas was about 45°, indicating an electrically homogeneous medium. From the fifth day, $\alpha_{max} > 70°$ for area A, and $\alpha_{max} < 30°$ for area B. Cracks then reached the second pseudodepth. It can be seen that the orientation of the main cracks was preserved through time and depth.

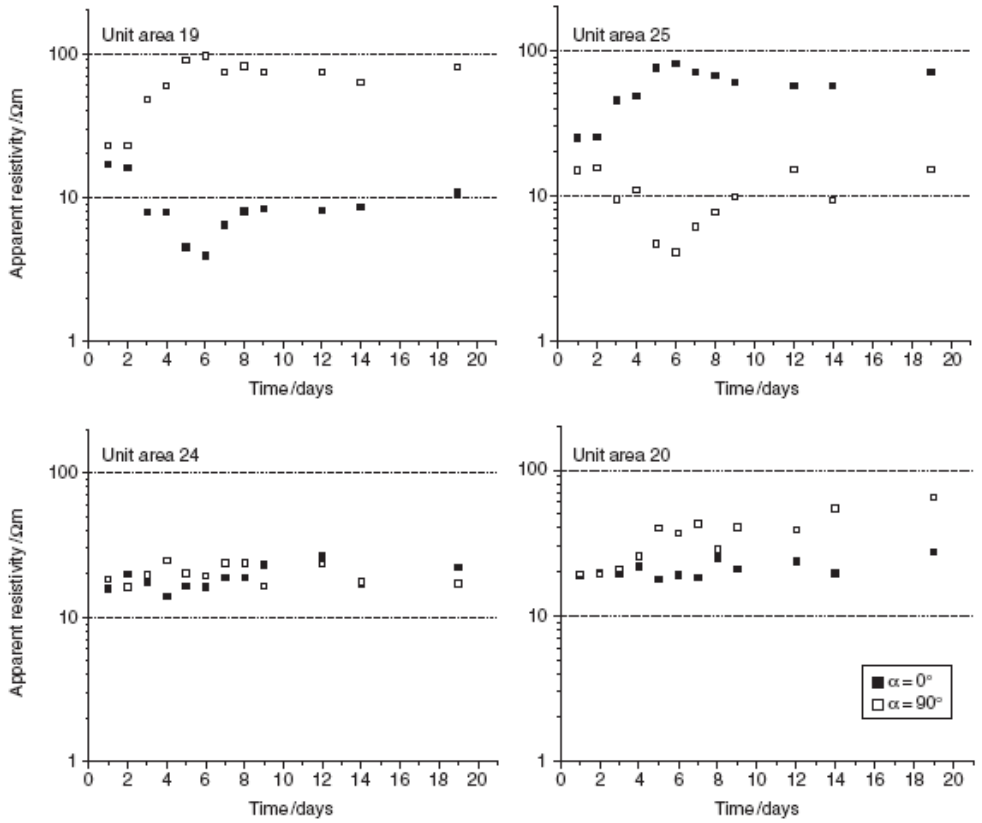

Figure 11 Apparent resistivity monitoring over 18 days, for the four unit areas 19, 25, 24 and 20 and at the first pseudo-depth.

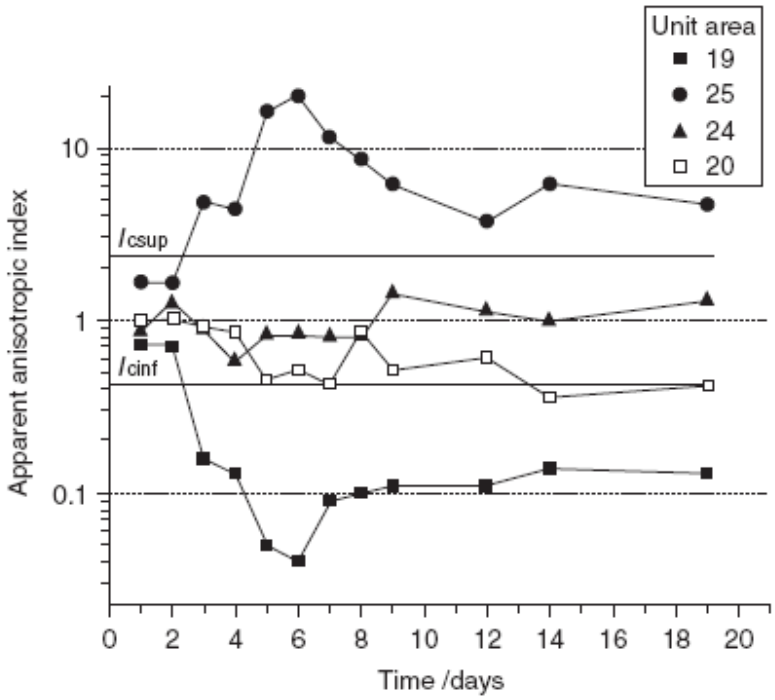

Figure 12 Variation of AAI and comparison with Icinf and Icsup thresholds during drying for the four unit areas 19, 25, 24 and 20.

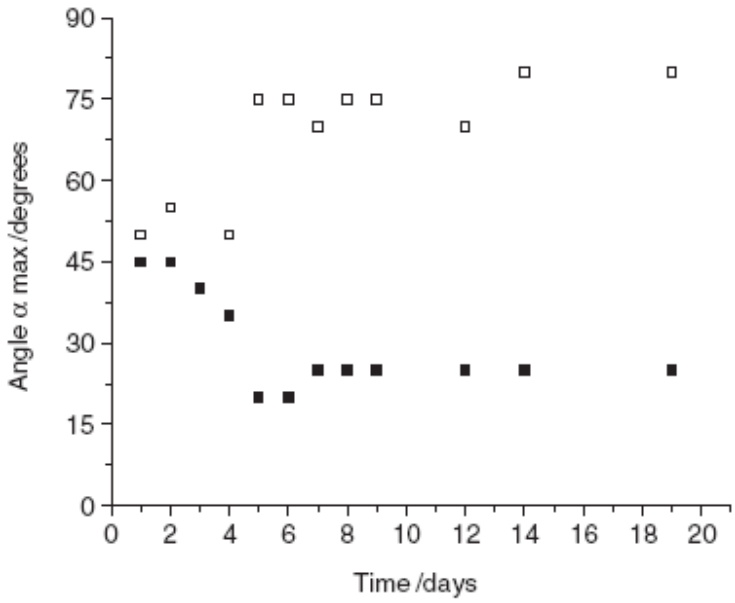

Figure 13 Orientation ofheterogeneit y for the second pseudo-depth, and during drying for the two areas A (&) and B (&) corresponding, respectively, to unit areas 17, 18, 24, 25; and 19, 20, 26, 27.

Conclusion

As expected, our results indicate that the measurements of electrical resistivity depend on electrical heterogeneity and that variations in the signal were detectable, even at this scale. These measurements also enabled us to monitor the development of cracking patterns during drying. The I_{cinf} and I_{csup} thresholds resulting from the apparent anisotropic index AAI and the orientation o the α_{max}-array are two methods useful for detecting electrical heterogeneities. The first was calculated for a specific electrical device, related to a specific soil texture and experimental conditions, and was applied for the first pseudo-depth. Nevertheless, it can be applied to the other temporal stages of drying. The second method took longer, but it has the advantage that it can be applied to the entire volume of the soil. The calculation of these two indexes gives an idea of the structure of the medium prior to data inversion. Indeed, it provided information on the presence, position, and extension of the cracks. The variation of these two indexes over time helps to explain how cracks develop. Nevertheless, neither method can distinguish units where cracks are oriented close to α = 45°, cracks that do not cross the in-line measurement MN, or non-cracked units. In future experiments, measurements along the diagonal could also be done. This would increase the acquisition time needed by about 20 minutes but would help to detect cracks oriented at 45°.

Acknowledgements : We are grateful to Keith Hodson for improving the original English text.

References

Bibby, H.M. 1986. Analysis ofmultiple-so urce bipole-quadripole resistivity surveys using the apparent resistivity tensor. Geophysics, 51, 972–983.

Chambers, J.E., Oglivy, R.D., Kuras, O., Cripps, J.C. & Meldrum, P.I. 2002. 3D electrical imaging ofknown targets at a controlled environmental test site. Environmental Geology, 41, 690–704.

Cousin, I., Levitz, P. & Bruand, A. 1996. Three-dimensional analysis of a loamy-clay soil using pore and chord distribution. European Journal of Soil Science, 47, 439–452.

Habberjam, G.M. & Watkins, G.E. 1967. The use of a square configuration in resistivity prospecting. Geophysical Prospecting, 15, 445–467.

Hallaire, V. 1988. La fissuration d'un sol argileux au cours du dessèchement. I. Description in situ. Agronomie, 8, 139–145.

Macedo, A., Crestana, S. & Vaz, C.M.P. 1998. X-ray microtomography to investigate thin layers ofs oil clod. Soil and Tillage Research, 49, 249–253.

Meheni, Y., Gue´ rin, R., Benderitter, Y. & Tabbagh, A. 1996. Subsurface DC resistivity mapping: approximate 1-D interpretation. Journal of Applied Geophysics, 34, 255–270.

Oglivy, R., Meldrum, P. & Chambers, J. 1999. Imaging of industrial waste deposits and buried quarry geometry by 3-D resistivity tomography. European Journal of Environmental and Engineering Geophysics, 3, 103–113.

Richard, G., Sillon, J.F. & Marloie, O. 2001. Comparison of inverse and direct evaporation methods for estimating soil hydraulic properties under different tillage practices. Soil Science Society of America Journal, 65, 215–224.

Ringrose-Voase, A.J. & Sanidad, W.B. 1996. A method for measuring the development of surface cracks in soils : application to crack development after lowland rice. Geoderma, 71, 245–261.

Samouelian, A., Cousin, I., Richard, G., Tabbagh, A. & Bruand, A. 2003. Electrical resistivity imaging for detecting soil cracking at the centimetric scale. Soil Science Society of AmericaJourna l, 67, 1319–1326.

Scollar, I., Tabbagh, A., Hesse, A. & Herzog, I. 1990. Archaeological Prospecting and Remote Sensing. Cambridge University Press, Cambridge.

Stengel, P. 1988. Cracks formation during swelling : effect on soil structure regeneration after compaction. In : Tillage and Traffic in Crop Production, pp. 147–152. Proceedings of the 11th International Conference of the International Soil Tillage Research Organization.
ISTRO, Haren, The Netherlands.

Tabbagh, A., Dabas, M., Hesse, A. & Panissod, C. 2000. Soil resistivity : a non-invasive tool to map soil structure horizonation. Geoderma, 97, 393–404.
Vogel, H.J., Weller, U. & Babel, U. 1993. Estimating orientation and width of channe ls and cracks at soil polished blocks – a stereological approach. Geoderma, 56, 301–316.
Xu, B. & Noel, M. 1993. On the completeness of data sets with multielectrode systems for electrical resistivity survey. Geophysical Prospecting, 41, 791–801.
Zhou, Q.Y., Shimada, J. & Sato, A. 2002. Temporal variations of the three-dimensional rainfall infiltration process in heterogeneous soil. Water Resources Research, 38, 1–16.